Lateral dispersion of dye and drifters in the center of a very large lake

Jun Choi[1], Cary Troy[2], Nathan Hawley[3], Michael McCormick[4], Mathew Wells[5]

Corresponding author: Cary Troy[2]

[1]Ocean Circulation and Climate Change Research Department

Korea Institute of Ocean Science and Technology

385, Haeyang-ro, Yeongdo-gu

Busan, Republic of Korea

jchoi@kiost.ac.kr

[2]Lyles School of Civil Engineering

Purdue University

550 Stadium Mall Drive

West Lafayette, IN 47907, U.S.A.

troy@purdue.edu

[3]Great Lakes Environmental Research Laboratory
4840 S. State Road
Ann Arbor, MI 48108
nathan.hawley@noaa.gov

[4]Cooperative Institute for Great Lakes Research
University of Michigan
G110 Dana Building
440 Church Street
Ann Arbor, MI 48109-1041
mccormmj@umich.edu

[5]Dept. of Physical and Environmental Sciences
University of Toronto - Scarborough
1265 Military Trail
Toronto, Ontario M1C 1A4, Canada
wells@utsc.utoronto.ca

Abstract

To better understand lateral dispersion of buoyant and non-buoyant pollutants within the surface waters of large lakes, two lateral dispersion experiments were carried out in Lake Michigan during the stratified period: (1) a dye tracking experiment lasting one day; and (2) a drifter tracking experiment lasting 24 days. Both the dye patch and drifters were surface-released at the center of Lake Michigan's southern basin. Near-surface shear induced by near-inertial Poincaré waves in enhancing lateral dispersion explains elevated dye dispersion rates (1.5 - 4.2 $m^2 s^{-1}$). During the largely windless first 5 days of the drifter release, the drifters exhibited nearly scale-independent dispersion ($K \sim L^{0.2}$), with an average dispersion coefficient of 0.14 $m^2 s^{-1}$. Scale-dependent drifter dispersion ensued after 5 days, with $K \sim L^{1.09}$ and corresponding dispersion coefficients of 0.3 - 2.0 $m^2 s^{-1}$ for length scales $L =$ 1500 - 8000 m. The largest drifter dispersion rates were found to be associated with lateral shear-induced spreading along a thermal front. Comparisons with other systems shows a wide range of spreading rates for large lakes, and larger rates in both the ocean and the Gulf of Mexico, which may be caused by the relative absence of submesoscale processes in offshore Lake Michigan.

Introduction

Accurate predictions of lateral dispersion in large enclosed and semi-enclosed water bodies are important for a wide range of applications including contaminant spills (Olascoaga and Haller 2012), algal blooms (Rowe et al. 2016), larval fish advection (Beletsky et al. 2007), invasive species (Beletsky et al. 2017) and microplastics (Hoffman and Hittinger 2017). With the increasing application of particle tracking models to simulate dispersion, direct measurements of dispersion in aquatic systems are becoming essential because the data provide a baseline against which these simulations can be compared, in turn allowing for model validation, calibration, and improvement. Additionally, direct measurements of dispersion can highlight linkages between dispersion and specific underlying physical processes, and these linkages can guide model refinement, leading to improved predictions. Despite the importance of dispersion for modelling many aquatic processes, there is a paucity of studies that constrain the magnitude of the dispersion processes within large lakes, or that distinguish between the dispersion of buoyant versus non-buoyant pollutants within the surface waters of lakes.

The focus of this work is on the lateral near-surface, offshore dispersion observed in Lake Michigan, USA (Figure 1), one of the Laurentian Great Lakes, which shares dynamical characteristics with many very large enclosed lakes and semi-enclosed ocean basins that are strongly influenced by the earth's rotation, largely free of tidal influence, primarily wind-driven, and density-stratified during most of the year. Very large basins (>100 km horizontal scale) that share these characteristics include the other Laurentian Great Lakes (Lakes Erie, Huron, Superior, and Ontario), Lake Baikal, Lake Victoria, Great Slave Lake, Great Bear Lake, Lake Winnipeg, the Caspian Sea, the Black Sea, the Mediterranean Sea, the Baltic Sea, and the Gulf of Mexico.

Estimating a lateral dispersion rate K is one key objective of dispersion studies in oceans and large lakes. It has important implications for the modeling and prediction of transport and mixing, particularly when it can be linked with the necessary mixing coefficients for numerical models (Peeters and Hoffman 2015, hereafter PH2015). In this paper we follow an unambiguous definition of the instantaneous dispersion rate K as the time rate of change of the lateral variance of the cloud or cluster σ^2 (exact definition follows later; see PH2015 for a comprehensive discussion on the relative merits of various dispersion coefficients). For molecular diffusion, K is invariant with time, producing linear variance growth $\sigma^2 \sim t$, but dispersion in natural waters generally exhibits "super-diffusion" for which the effective dispersion rate K increases with the size of the cloud, and therefore time as well. There are several established mechanisms that lead to a length scale dependence of the dispersion coefficient.

Drifter and dye experiments (Okubo 1971; Murthy 1976; Koszalka et al. 2009; Lumpkin and Elipot 2010; Poje et al. 2014) have supported the celebrated oceanic scale-dependent parameterization for K, Richardson's 4/3 power law (Richardson 1926), for which $K \sim \sigma^{4/3}$, and an associated cluster variance that grows as $\sigma^2 \sim t^3$. The 4/3 power law is expected to hold in homogeneous, isotropic stationary turbulence when the velocity (energy) spectrum exhibits a well-defined -5/3 decay in the inertial subrange and the cloud size falls within the inertial subrange scales (Batchelor 1950).

The presence of background horizontal and vertical shear can also elevate lateral dispersion rates; this shear can also lead to scale-dependent lateral dispersion (Fischer et al. 1979). Drifter and dye studies carried out in lakes have linked horizontal and vertical shear to observed size-dependent dispersion (Lawrence et al. 1995; Peeters et al. 1996; Stocker and Imberger 2003; Choi et al., 2015; PH2015), and shear may be the dominant spreading mechanism in the surface waters of lakes, for which the lateral turbulence field is unlikely to be well-developed given the ephemeral nature of wind forcing. Recent work has shown wind-induced vertical shear within 1 m of the water surface to greatly enhance lateral spreading of near-surface substances, even in very light winds (Laxague et al., 2017).

Recent oceanic drifter studies have highlighted linkages between surface dispersion and submesoscale currents (Poje et al. 2014; Lumkin and Elipot 2010). Submesoscale currents are defined as motions having length scales of ~100 m - 10 km and time scales of hours to days, respectively, and are often associated with lateral buoyancy gradients and fronts (Thomas et al. 2008; McWilliams 2016). Submesoscale features have not been identified or examined in large lakes, such as the Laurentian Great Lakes, although eddy- and front-like features are sometimes observed in satellite synthetic aperture radar (SAR) imagery (McKinney et al. 2012; Ralph 2002) and in the patterns of resuspension plumes (Lee et al. 2007; Eadie et al. 2008) and chlorophyll-a plumes (Kerfoot et al. 2008).

We are not aware of any dispersion measurements performed outside of the coastal boundary layer in lakes with sizes comparable to the largest Laurentian Great Lakes (basin widths $\gtrsim$100 km); importantly, without such measurements, it is unclear whether the magnitude of offshore dispersion in lakes of such size is more similar to smaller lakes, enclosed and semi-enclosed seas, or the open ocean.

In this paper we present measurements of drifter and dye dispersion from experiments carried out in the surface waters at the center of Lake Michigan's southern basin during the stratified period. The dye patch was surface-released and tracked for approximately one day; 6 drifters were co-released and tracked for 24 days, during which they remained in the interior waters of the basin.

The main research questions addressed in this work are 1) what dispersion rates are observed in the interior surface waters of a very large lake, and how do they compare with other observations? 2) are there differences between the dispersion of dye and drifters? and 3) how do these observations relate to resolvable physical processes? This paper is outlined as follows: in the Methods section we describe the experiments and dispersion quantification techniques; in the Results section we present the observed dispersion rates as well as the physical conditions during the experiment; and in the Discussion section we relate our observations to resolvable physical processes and other lake and ocean observations.

Methods

We collected and analyzed a set of field measurements taken in Lake Michigan, from June-August of 2013 (Figure 1). The location for all of these measurements was the center of Lake Michigan's 135 km wide southern basin, where water depths reach 153 m, and near-inertial waves dominate surface currents during the stratified period (Choi et al. 2012). The measurements consisted of: (1) water column velocities and temperatures from an acoustic Doppler current profiler (ADCP) and a thermistor string; (2) surface wave and meteorological observations from nearby NDBC Buoy 45007; (3) a surface dye release near this same location, which was tracked for slightly more than 1 day; (4) a simultaneous release of a drifter cluster that was subsequently tracked for ~100 days. For this manuscript, we focus on measurements from the 24 day-period DOY 195-219 (14 July 2013 – 7 August 2013), during which the drifter cluster remained in the interior of the lake, and outside the coastal boundary layer.

Water currents and temperatures were measured continuously at a mid-lake mooring (42 42' 30" N, 87 3' 52" W) that was deployed from DOY 160-256 of 2013. This mooring included a RDI

Workhorse 307.2 kHz ADCP in an up-looking configuration that sampled currents in 1 m bins every 20 min, between 4.9 and 39.9 m depth. Subsurface temperatures were measured by a dense array of thermistors, with 37 temperature loggers (Sea Bird SBD-56 and RBR TR-1060) located between 11 and 41 m depth. During the dye release experiment, high resolution CTD casts were performed to quantify near-surface thermal structure and possible overturning. Wind, wave, and surface temperature data was obtained from NDBC Buoy 45007, which was located 5.6 km from our mooring (Figure 1).

A dye release experiment was conducted on 14 July 2013 (DOY 195) near the mooring location during a R/V Blue Heron cruise that took place from 14 July 2013 to 18 July 2013. A dye mixture was prepared using 11 kg Rhodamine WT, 70% ethanol alcohol, and *in situ* surface water. The density of the dye mixture was measured with a benchtop densimometer (Mettler Toledo DE45) to be 997.1 $kg\,m^{-3}$, which was slightly less dense than the lake surface water, which had an estimated density of 999.9 $kg\,m^{-3}$.

To inject the dye into the surface waters of the lake, the dye mixture was pumped from a barrel into the surface water for 8 minutes through a surface diffuser. The surface diffuser was a 0.5 m long floating section of 15 cm diameter plastic pipe with several hundred 2 mm diameter holes. The dye was pumped through the diffuser while the ship drifted, approximately 30 m distant from the diffuser. The resulting initial dye patch was an elongated dye streak approximately 200 m long and 30 m wide. Following the completion of the dye injection, the ship drifted away from the dye patch without engaging the propellers in order to avoid disturbing the patch.

The dye concentration was spatially mapped by traversing the ship at 3.6 ms^{-1}through the dye patch, without engaging the propellers, and measuring the surface water dye concentrations with a calibrated Turner 10-AU fluorometer connected to the ship's underway water system (2 m depth). The estimated detection level of the fluorometer is 0.01 μgL^{-1}, which restricted the dye experiment duration to approximately one day, after which the dye patch could not be detected. We have limited information on the vertical extent of the dye patch due to the very weak vertical mixing during the release; our towed fluorometer, which was towed as shallow as 3 m, did not detect any dye, which at least confirmed the surface-trapped location of the plume.

One hour following the dye release, 6 GPS-based drifters were released from the ship into the center of the dye patch during one of the measurement transects through the patch (Supplemental Material, Animation S1). The drifters were designed after the "Eddie" type drifter described by NOAA's Northeast Fisheries Science Center (https://www.nefsc.noaa.gov/epd/ocean/MainPage/lob/driftdesign.html). They are a spar type drifter with the buoyancy concentrated near the top of the spar and an overall length of 1.2 m. A cruciform drogue of approximately 1 m^2 area is attached to the spar. This design is similar to CODE-type drifter, which performs virtually in the same manner with newly designed CARTHE drifters (Lumpkin et al. 2017). At the very top is a 0.1 m by 0.18 m platform with an attached North Star TrackPack GPS. These units have horizontal positioning accuracy of less than 5 m and hourly position updates. The main buoyancy is comprised of 4 small floats of about 0.9 kg of buoyancy each and 3.6 kg of lead ballast attached near the base of the spar. The total mass of the drifter in air is about 5 kg. Six drifters remained in Lake Michigan's southern basin for 3 months, but we restrict the discussion here to data associated with the first 24 days of the drifter experiment, during which the drifters remained offshore before being entrained into the coastal boundary layer.

The drifter cluster size was quantified using standard definitions of position variance. The variance of the drifter displacements was quantified as $\sigma_{ij}^2 = 2\sigma_i\sigma_j$, where σ_i and σ_j are standard deviations of drifter positions in major and minor axes, respectively, which were determined by principal axis analysis (Okubo 1971). Drifter velocities were calculated using the time derivatives of the drifter horizontal positions, and for the dye release we estimated the bulk velocity shear over the top 5m of the water column by taking the difference between the average drifter (surface) velocities and the ADCP measurement at 4.9 m depth.

For the dye plume, ordinary Kriging interpolation was used to estimate the spatial distribution of the dye plume concentrations from the ship-based fluorometer measurements $c(x,y)$, from which the variance of the dye concentration distribution was calculated as $\sigma_{ij}^2 = 2\sigma_i\sigma_j$. Here σ_i and σ_j are the standard deviations the dye distribution along major and minor plume axes, respectively, which were estimated following the covariance matrix eigenvalue technique described in Peeters et al. (1996). We have chosen to analyze the period 6-20.6 h following dye release in order to avoid any potential errors associated with either ship-induced mixing (early times) or sparsely – mapped distributions (late times), following suggestions from reviewers.

The instantaneous dispersion rate for both dye and drifters is defined as $K = \frac{1}{4}\frac{d\sigma_{ij}^2}{dt}$, which we choose as our metric of dispersion because it avoids issues with the unknown initial cluster size, time origin, and the integration of different phases of dispersion into a single coefficient (PH2015). The overall cluster/plume size is defined as $L = 3\sigma_{ij}$.

To further examine the role of vertical shear in the enhancement of the lateral dye dispersion, we performed data-driven particle tracking to simulate the growth of the dye cloud (see Choi et al. 2015 for further details on the technique). For the simulations, the lateral diffusion coefficient was set to the measured, approximately constant value experienced by the drifters during the first 5 days of the experiment (0.14 m^2s^{-1}). The vertical shear was specified according to the combined drifter-ADCP estimate, and the vertical diffusivity held constant. The initial condition for the simulations was taken to be the measured dye cloud variance several hours after release, as a precaution to ensure that any ship-induced mixing of the dye cloud was not considered.

Observations

Background conditions

The wind stress, currents, and thermal structure measured by the mooring and NDBC Buoy 45007 during DOY 195-220 in 2013 are highlighted in Figure 3. During the first five days of the drifter deployment (DOY 195-DOY 200), which includes the day-long dye release experiment (DOY 195-196), winds were calm, with a mean estimated stress of 0.017 Pa (the mean June-July wind stress is 0.03 Pa for Buoy 45007, for comparison). The largest wind event of the 24 day period was an event on DOY 205, which had a maximum stress of 0.4 Pa; this event created significant wave heights in excess of 3 m and significantly deepened the mixed layer (Figure 3c). The mean wind stress for the entire 24 day period was 0.056 Pa, but quite variable with a standard deviation of 0.062 Pa, as can be seen in Figure 3.

The stratification of surface waters evolved during the start of the experiment in response to changing winds. Initially there was from a weakly stratified system, which changed to a well-formed mixed layer following the large wind event just described (Figure 3c). The buoyance frequency, a measure of density stratification, over the top 15 m of the water column is calculated as $N = 1 \times 10^{-3}$ rads^{-1} (0.58 $^{\circ}$Cm^{-1}) from DOY 190 – 205, and $N = 9 \times 10^{-5}$ rads^{-1} (0.05 $^{\circ}$Cm^{-1}) from DOY 205 – 220. During the dye release (DOY 205), stratification extended to within 1 m of the lake surface (Figure 4), suggesting very weak vertical mixing (discussed later).

Lake Michigan surface water temperatures obtained from satellite imagery (https://coastwatch.glerl.noaa.gov/) showed that during the measurement period the southern basin had a strong north-south temperature gradient with warmer southern waters, with an average of 1.05 ℃ higher temperature at a location of 50 km to the south of the drifter release location. Associated with this persistent north-south gradient in lake surface temperature was a strong thermal front that we highlight later as potentially playing a role in the observed drifter trajectories and spreading.

Measured currents from both the drifters and the ADCP show the dominance of near-inertial energy in near-surface and surface currents (Figures 3c, 4). Near-inertial surface currents experienced by the drifters nearly reached 0.5 ms^{-1}, rotating clockwise at near-inertial period (~18 h), as we have shown previously for this location in Lake Michigan (Choi et al. 2012, 2015). The largely near-inertial current field is also seen to be non-stationary, which is a product of the temporal structure of the wind forcing (Figure 3a). The drifters maintained more than 80% coherence at the inertial frequency for the duration of the period shown (Figure 4), which confirms the large spatial scale associated with the dominant internal near-inertial Poincaré wave (Ahmed et al., 2012), and the lateral uniformity of the near-inertial currents.

Conditions during the dye release

The surface conditions during the dye release were very calm, with mean wind stress of 0.004 Pa and a mean wave height of 0.1 m (Figure 5). Thermal stratification extended to 1 m below the surface, our shallowest measurement depth. The strength of this near-surface stratification between 1 and 7 m depth was $N = 2.7 \pm 0.5 \times 10^{-2}$ rads^{-1} during the 21 hour experiment. Shear estimated at 2.5 m depth is clearly dominated by near-inertial waves (Figure 5), which is consistent with the surface velocities (Figures 3c,4). The corresponding Richardson numbers estimated at 2.5 m depth did not fall below 1 during the dye release.

Analysis of the micro-temperature profiles measured by the SCAMP (Self Contained Autonomous Microstructure Profiler) taken during the dye release, and the several days following the release (which had a similar lack of wind forcing), revealed that Thorpe overturn scales (L_t) between 1 and 7 m depth were less than our minimum detection scale of 2 cm on average. A mixing efficiency approach (Scotti 2015) yields a vertical mixing coefficient of $K_z \approx 3 \times 10^{-6}$ m^{2}s^{-1} as a generous upper bound on the vertical mixing coefficient between 1 and 7 m depth. This low level of mixing below 1 m is consistent with the consistent presence of stratification during the dye release, and with Richardson numbers > 1 estimated at 2.5 m depth.

Within 1 m of the water surface we do not have direct measurements of thermal microstructure or velocity shear. However, if we assume that the weak winds were the cause of any turbulence within 1 m of the water surface, then a parabolic distribution for the turbulent coefficient yields $K_z \approx \frac{u_* \kappa h}{6} = 1.3 \times 10^{-4}$ m^{2}s^{-1} as an estimate of the average vertical mixing rate within 1 m. Here $u_* = 0.002$ ms^{-1} is the water side friction velocity associated with the wind stress (0.004 Pa), $\kappa = 0.4$ is von Karman's constant, and $h = 1$ m is the layer thickness over which the stress is assumed to decay (since the water column was strongly stratified to at least 1 m depth). This is likely an overestimate of the average near-surface mixing rate because (1) the layer thickness over which the wind stress was acting (assumed 1 m) may have been even smaller; and (2) some portion of the wind stress is expected to have gone into the development and growth of the wave field since waves were not developed during the dye release.

Dispersion observations

During the first day of the dye release, the drifter and dye clouds were observed to move in a clockwise trajectory consistent with the looping near-inertial currents, with a net center of mass displacement of 4 km over 21.6 h (Figure 6). The dye cloud exhibited nearly continuous growth, but the drifter cluster size was nearly constant, even decreasing, for the first 18 hours of the experiment (Figure 7). After 20.6 h, the dye cloud scale was $L = 3\sigma_{ij} = 2900$ m, whereas the drifter cluster size was only L = 374 m (Figures 6, 7), in spite of their similar initial cloud sizes and release times. The two distributions overlapped one another for the duration of the dye mapping experiment (Figure 6).

The dye cloud exhibited scale-dependent spreading, with spreading rates ranging from $K = 1.5$ - 4.2 m^2s^{-1} for times of 6 - 21 h following release, respectively, with an approximate scale dependency of $K \sim L^{0.97}$ (Table 1). In contrast, the drifter spreading over the first five days of the experiment was nearly scale-independent, with variance growth $K \sim L^{0.2}$, which is reasonably approximated with a scale-independent (constant) lateral dispersion coefficient of $K = 0.14$ m^2s^{-1}. After five days, the drifter cluster size was still only $L = 3\sigma_{ij} = 1460$m. As discussed previously, the first five days of the experiment had very low winds (Figure 3, Table 1).

The longer term drifter trajectories illustrate the "inertial waltzes" caused by the combination of low-frequency currents and clockwise-spiraling near-inertial currents (Mortimer 2004; Supplemental Material Animation S1 and Figure 8). These pathlines vary between nearly closed orbits (e.g. DOY 201 to 207) and straight lines (e.g. DOY 208), depending on the strength of near-inertial currents relative to non-rotating currents. The inertial circles become absent once the drifters reach the edge of the coastal boundary layer at the end of the period shown, since the coastal boundary layer is a location with strong alongshore flow and diminished near-inertial energy (DOY 219 - 220, Figure 8).

For experiment days 5-24, the drifter cluster grew according to $\sigma_{ij}^2 \sim t^{2.2}$, which is suggestive of scale-dependent super-diffusion ($\sigma_{ij}^2 \sim t^{>1}$). It cannot be determined whether this change to scale-dependent dispersion at t = 5 days occurred due to the cluster reaching a critical size threshold or due to the increased winds experienced for the period t > 5 days. The corresponding scale-dependent relation for the dispersion rate during this period is $K \sim L^{1.09}$, with a maximum value of 2.0 m^2s^{-1} after 24 days when $L = 8000$ m (Table 1).

Discussion

In addition to the direct quantification of lateral dispersion rates in a very large lake, the dye and drifter observations highlight several important features about near-surface dispersion characteristics in offshore waters of large lakes, including linkages to physical processes. We characterize the dispersion in terms of vertical shear, an observed thermal front, and scale-dependency relative to other systems.

Importance of vertical shear

Firstly, a comparison between the dye and drifter spreading rates (K) during the first day of the experiment provides additional evidence for the importance of near-surface vertical shear in enhancing lateral dispersion, differentiating surface drifter dispersion from near-surface dye dispersion, particularly for times immediately following release when scale-dependent dispersion has not yet occurred. Particle tracking calculations (Figure 10) show that vertical shear is a plausible mechanism to partially explain the enhanced, scale-dependent spreading experienced by the dye (Figure 10). While the particle tracking calculations do not entirely reproduce the larger variance growth experienced by the dye cloud, these calculations likely underestimate the shear effect as they are driven by a shear estimate averaged over the top 5 m of the water column (Figure 5), and therefore do not capture the enhanced near-surface, cm to m scale shear that Laxague et al. (2017) showed to greatly enhance near-surface spreading of dissolved substances even under weak winds. Because the resolved shear driving our calculations is primarily near-inertial (Figure 5), the most direct conclusion to be drawn from the particle tracking results is that near-inertial vertical shear can cause enhanced scale-dependent spreading of dissolved near-surface substances. The near-inertial spreading mechanism was previously examined in Choi et al. (2015), and operates in the absence of direct forcing from the wind, since the inertial waves have a decay time scale of approximately 10 days for Lake Michigan (Choi et al. 2012). Future studies measuring the near-surface spreading of dissolved substances should aim to also quantify the concurrent vertical shear as close to the water surface as possible.

Dispersion along a thermal front

A significant growth in the cluster size was associated with the travel of the drifters along a strong thermal front, which occurred during days 14-19 of the experiment (Figures 11, 12). Sea surface temperature (SST) imagery revealed that during this period, the drifters were traveling across a strong thermal front aligned in a northwest-southeast orientation. Based on SST imagery, the thermal front separated a large, warmer water mass in the southwestern part of the southern basin from a warmer mass to the north. At its strongest, the front was approximately 10 km wide, and cross-front thermal gradients ranged from 0.01-0.07 °Ckm^{-1} (Days 15-19; Figure 12). The drifters converged to the front, and then traveled southeast along the front until they reached and were entrained into the coastal boundary layer (Day 20). The orientation of the front was consistent but it migrated southward during the period when the drifters traveled along it (Figures 11,12), and a simple thermal wind dynamical balance applied to the front is consistent with the observed frontal speeds inferred from the drifters, i.e. 11 km in 4 days = 0.03 ms^{-1}.

The increase in the drifter cluster size seen during the frontal activity is a result of elongation along the major cluster axis, which suggests that shear associated with the frontal velocity field was the cause of the cluster elongation (Figure 12). In rotational systems, convergent thermal fronts are associated with convergence of surface waters and strong along-front velocities in the form of a jet that spans the location of the front (Cushman-Roisin and Beckers 2011, p. 592). In the northern hemisphere, the expected along-front velocity is in a direction such that cold water is on the left in the frame of the moving fluid, which is consistent with the front observed here (McWilliams 2016). Dynamically, the flow near fronts is typically explained (to lowest order) using a geostrophic balance and the thermal wind equation, where the cross-front pressure gradient provided by buoyancy balances the Coriolis force (McWilliams 2016). In addition to a strong magnitude of along-front flow (termed a “baroclinic jet”), fronts can be regions of strong cross-front and vertical shear, which to our knowledge has not been examined in the context of shear-enhanced dispersion.

The problem of along-front dispersion by cross-front shear is analogous to the classic problem of unbounded shear flow dispersion (Fischer et al. 1979; Saffman 1962). In true shear flow dispersion, longitudinal dispersion is enhanced in the flow direction as transverse diffusion allows fluid and substances to “sample” different velocities in the sheared profile (Fischer et al. 1979). For fronts that are not dynamically unstable, transverse diffusion across the front may be limited, and transverse motions further constrained by convergent velocities that return water to the front (for convergent fronts). As such, the process of enhanced dispersion along stable fronts may be best thought of as simple differential advection, analogous to the longitudinal spreading of fluid parcels over time on distinct conveyer belts that are traveling at different speeds. This is a limiting case of shear flow dispersion (negligible transverse diffusion), and actually the most dispersive according to basic theories. Without further knowledge of the cross-front shear in the baroclinic jet, it is difficult to quantify this effect further. However, if the drifter cluster was distributed evenly across the baroclinic jet and being advected differentially, in the four days during which the drifters travelled along the front, the expected differential advection experienced would be $\Delta x \sim \Delta v \Delta t \sim 5$ km, which shows that even the modest front observed in the present Lake Michigan study is sufficiently strong to substantially impact dispersion (due in large part to the low levels of dispersion experienced otherwise). As such, models seeking to faithfully represent surface dispersion in lakes with significant lateral extent should aim to correctly resolve thermal fronts resulting from differential heating.

Scale dependency and comparison to other systems

It is important to discuss the results in the context of the limited measurements available for the offshore regions of other large lakes and oceanic basins, for the purpose of extrapolating the results to other systems. As points of comparison we include the Lake Ontario dye data of Murthy (1976), recent Lake Constance drifter data from PH2015, the classic collected ocean dye dataset of Okubo (1971), and data from the recent GLAD drifter experiment from the Gulf of Mexico (Poje et al. 2014; https://data.gulfresearchinitiative.org/). The Gulf of Mexico was selected for comparison because while it is much larger than Lake Michigan, the two basins share important dynamical similarities, having weak tidal influence and strong near-inertial energy that dominates mixed layer currents. In order to facilitate comparison with the Lake Michigan drifters, we have re-computed GLAD S2 spreading statistics for 22 individual clusters of 4 drifters that had initial drifter separations less than 300 m. Lake Constance was also chosen although it is much smaller than

Lake Michigan because it is large enough to contain near-inertial energy that potentially affects the dispersion.

Figure 13 and Table 1 show the scale dependencies exhibited by the different systems and experiments, from which several observations can be made. Firstly, surface dye releases from Lake Ontario, Lake Michigan, and the ocean have larger dispersion rates than drifter data, which would seem to be additional confirmation of the vertical shear effect, since vertical shear affects dissolved substances but not floating objects. All of the dye data also show scale dependence of the dispersion coefficient even at small plume scales, which is consistent with the effect of vertical shear on spreading.

A comparison of our Lake Michigan drifter data with the results from PH2015 for the smaller Lake Constance also highlights some interesting features. Firstly, the Lake Constance data shows scale dependence at smaller scales (10^2-10^3 m) than the Lake Michigan data (10^3 m), in spite of the elevated overall surface energy level in Lake Michigan (LM surface velocities approaching 0.5 ms^{-1}, Figure 4, as opposed to 0.1 ms^{-1} for Lake Constance). One key difference between the experiments is the season during which they were conducted: the Lake Constance experiments were carried out when the water column was very weakly stratified (Feb, March), whereas our own experiments were conducted when the lake was strongly stratified (July). The two sets of data had similarly low wind speeds, averaging $\lesssim 5ms^{-1}$, but stratified Lake Michigan is known to very efficiently absorb wind energy into the fundamental near-inertial internal seiche, to the point where velocities are nearly tide-like in their periodicity (Choi et al., 2012, shown herein in Figure 4). In contrast, wind will be more efficiently transferred to dispersion-enhancing surface eddies in an unstratified lake, potentially leading to scale-dependent spreading at smaller plume scales.

It may also be that in smaller lake, lateral shear is elevated due to the diminished basin size, where the nearshore boundary layer occupies a larger fraction of the lake area.

Perhaps most importantly, the comparison in spreading rates between the Lake Constance drifter experiments and our present Lake Michigan data show that that there is no universal "diffusion diagram" for large lakes, or even a single lake; this is best proved by examining the Lake Constance data on its own, which shows four very distinct curves for very similar forcing and background conditions. Beyond seasonal differences, this variability is largely a function of the high degree of non-stationarity associated with lakes, which are driven by highly variable winds, in contrast to larger ocean basins. As such, the key elements causing dispersion – vertical/lateral shear and turbulent eddies – are more highly variable in space and time. This variability also means that any one large lake dispersion experiment should be viewed as merely one possible realization of many possible experiments, and even a single experiment can sample different dispersion regimes, as can be seen by comparing the spreading behavior for our drifters between the largely windless first five days and the remainder of the experiment.

In spite of the dynamical similarities between Lake Michigan and the Gulf of Mexico, the Gulf drifter spreading rates are an order of magnitude larger than Lake Michigan, and also exhibit scale dependence at smaller scales. With the Lake Constance verses Lake Michigan comparison dispelling the notion that "larger lakes have larger dispersion rates", it may still be correct that (larger) semi-enclosed ocean basins have larger dispersion rates than lakes. One hypothesis to explain this idea is that large lakes with energetic near-inertial waves lack the energetic submesoscale motions that have been shown to play an important role in oceanic lateral dispersion (Poje et al. 2014, and Lumkin and Elipot 2010). Submesoscale structures have length scales from about 100 m to 10 km, and are generated by mixed layer instability, lateral shear, lateral buoyancy gradients, and other mechanisms (McWilliams 2016). They can enhance lateral dispersion both directly and indirectly, as they feed energy to larger scale motions through an inverse energy cascade (LaCasce 2008).

Submesoscale features have not been examined in large lakes, although many of the necessary precursors to their existence – including fronts, as seen in the present experiment – are present. Submesoscale activity is generally larger for larger surface buoyancy gradients, and while Lake Michigan lacks a substantial riverine input during the summer, onshore-offshore and north-south thermal gradients can exist in surface waters due to gradients in water depth and meteorological forcing. Additionally, upwelling events can generate lateral buoyancy gradients along upwelling fronts. Without more detailed measurements it is difficult to assess whether the thermal front seen in our Lake Michigan experiment was unstable, but the observed low rates of cross-front cluster spreading seems to suggest that the front was not unstable. Thus, while some of the necessary precursors to submesoscale activity seem to be present in large lakes, further work is necessary to quantify the possible generation and existence of submesoscale motions in large lakes.

Conclusions

The data presented here have important implications for the modeling and prediction of lateral surface transport and dispersion in the offshore waters of large lakes and enclosed basins. The data have highlighted several physical mechanisms important to lateral dispersion, as well as similarities and differences between oceanic dispersion – for which much more is known – and large lake dispersion. In particular our results of dye and drifter experiments suggested that the dispersion rate for dissolved substances is augmented in the presence of near-inertial, near-surface shear, and that very near surface shear may contribute additional enhancement, following recent findings by Laxague et al. (2017). Lateral shear from a thermal front was also found to enhance lateral spreading, and these observations suggest the need to resolve both vertical and lateral shear in models aiming to accurately simulate the lateral dispersion of substances in lakes, which is consistent with earlier ideas from PH2015 and Choi et al. (2015).

Our results herein help to span an important observational gap related to the offshore dispersion of substances in very large lakes (basin scales > 10^2 km) and observations in both smaller lakes and larger oceans. Our observed Lake Michigan dispersion rates fall closer to those observed in smaller lake (Lake Constance, PH2015), and exhibit neither the magnitude nor the robust scale-dependence seen in ocean and Gulf of Mexico observations. We hypothesize that this is due in part to the ephemeral, non-stationary nature of wind forcing in lakes, as well as a related consistent lack of submesoscale energy. These hypotheses deserve attention in future studies.

Acknowledgements

This material is based upon work that was supported by the National Science Foundation, Division of Ocean Sciences, Physical Oceanography Program (Grant OCE-1030842). The authors are also grateful to the captains and crews of the R/V Blue Heron (UNOLS) and R/V Laurentian (NOAA-GLERL), as well as David Cannon, William Schmidt, and Mijanur Chowdhury for help with the instrumentation and field work. Several anonymous reviewers provided constructive feedback for which we are also very grateful.

References

Ahmed, S., C. D. Troy, and N. Hawley. 2013. Spatial structure of internal Poincaré waves in Lake Michigan, Environmental Fluid Mechanics, 1–21. doi:10.1007/s10652-013-9294-3

Batchelor, G. 1950. The application of the similarity theory of turbulence to atmospheric diffusion. Quarterly Journal of the Royal Meteorological Society, 76, 133–146. doi: 10.1002/qj.49707632804

Beletsky, D., Beletsky, R., Rutherford, E.S., Sieracki, J.L., Bossenbroek, J.M., Chadderton, W.L., Wittmann, M.E., Annis, G.M. and Lodge, D.M. 2017. Predicting spread of aquatic invasive species by lake currents. Journal of Great Lakes Research, 43(3), pp.14-32. doi:10.1016/j.jglr.2017.02.001

Beletsky, D., Mason, D. M., Schwab, D. J., Rutherford, E. S., Janssen, J., Clapp, D. F., and Dettmers, J. M. 2007. Biophysical model of larval yellow perch advection and settlement in Lake Michigan. Journal of Great Lakes Research, 33(4), 842-866. doi:10.3394/0380-1330(2007)33[842:BMOLYP]2.0.CO;2

Choi, J., C. D. Troy, T.-C. Hsieh, N. Hawley, and M. J. McCormick. 2012. A year of internal Poincaré waves in southern Lake Michigan, Journal of Geophysical Research: Oceans, 117: C07014. doi:10.1029/2012JC007984

Choi, J. M., Troy, C. D., and Hawley, N. 2015. Shear dispersion from near-inertial internal Poincaré waves in large lakes. Limnology and Oceanography, 60(6), 2222-2235. doi: 10.1002/lno.10163

Cushman-Roisin, B. and Beckers, J.M., 2011. Introduction to geophysical fluid dynamics: physical and numerical aspects. Academic press.

Eadie, B. J., Robbins, J. A., Klump, J. V., Schwab, D. J., and Edgington, D. N. 2008. Winter-spring storms and their influence on sediment resuspension, transport, and accumulation patterns in southern Lake Michigan. Oceanography, 21(4), 118-135. doi:10.5670/oceanog.2008.09

Fischer, H., E. List, R. Koh, J. Imberger, and N. Brooks. 1979. Mixing in inland and coastal waters, Academic.

Hoffman, M.J. and Hittinger, E. 2017. Inventory and transport of plastic debris in the Laurentian Great Lakes. Marine pollution bulletin, 115(1), pp.273-281. doi:10.1016/j.marpolbul.2016.11.061

Kerfoot, W. C., Budd, J. W., Green, S. A., Cotner, J. B., Biddanda, B. A., Schwab, D. J., and Vanderploeg, H. A. 2008. Doughnut in the desert: Late-winter production pulse in southern Lake Michigan. Limnology and Oceanography, 53(2), 589. doi:10.4319/lo.2008.53.2.0589

Koszalka, I., LaCasce, J. H., and Orvik, K. A. 2009. Relative dispersion in the Nordic Seas. Journal of Marine Research, 67(4), 411-433. doi:10.1357/002224009790741102

LaCasce, J. H. 2008. Statistics from Lagrangian observations. Progress in Oceanography, 77(1), 1-29. doi:10.1016/j.pocean.2008.02.002

Laxague, N.J., Özgökmen, T.M., Haus, B.K., Novelli, G., Shcherbina, A., Sutherland, P., Guigand, C.M., Lund, B., Mehta, S., Alday, M. and Molemaker, J., 2018. Observations of near-surface current shear help describe oceanic oil and plastic transport. Geophysical Research Letters, 45(1), pp.245-249. doi: 10.1002/2017GL075891

Lawrence, G. A., Ashley, K. I., Yonemitsu, N., and Ellis, J. R. 1995. Natural dispersion in a small lake. Limnology and Oceanography, 40(8), 1519-1526. doi:10.4319/lo.1995.40.8.1519

Lee, C., Schwab, D. J., Beletsky, D., Stroud, J., and Lesht, B. 2007. Numerical modeling of mixed sediment resuspension, transport, and deposition during the March 1998 episodic events in southern Lake Michigan. Journal of Geophysical Research: Oceans, 112(C2). doi:10.1029/2005JC003419

Lumpkin, R., and Elipot, S. 2010. Surface drifter pair spreading in the North Atlantic. Journal of Geophysical Research: Oceans, 115(C12). doi:10.1029/2010JC006338

Lumpkin, R., Özgökmen, T. and Centurioni, L. 2017. Advances in the application of surface drifters. Annual Review of Marine Science, 9, pp.59-81. doi:10.1146/annurev-marine-010816-060641

McKinney, P., Holt, B., and Matsumoto, K. 2012. Small eddies observed in Lake Superior using SAR and sea surface temperature imagery. Journal of Great Lakes Research, 38(4), 786-797. doi:10.1016/j.jglr.2012.09.023

McWilliams, J.C., 2016. Submesoscale currents in the ocean. Proceedings of the Royal Society A: Mathematical, Physical and Engineering Sciences, 472(2189), p.20160117. doi:10.1098/rspa.2016.0117

Mortimer, C. H. 2004. Lake Michigan in Motion-Responses of an Inland Sea to Weather, Earth-Spin, and Human Activities, The University of Wisconsin Press.

Murthy, C. 1976. Horizontal diffusion characteristics in Lake Ontario. Journal of Physical Oceanography, 6: 76–84. doi:10.1175/15200485(1976)006 < 0076:HDCILO>2.0.CO;2

Okubo, A. 1971. Oceanic diffusion diagrams, Deep sea research and oceanographic abstracts, Elsevier, 789–802. doi:10.1016/00117471(71)90046-5

Olascoaga, M.J. and Haller, G., 2012. Forecasting sudden changes in environmental pollution patterns. Proceedings of the National Academy of Sciences, 109(13), pp.4738-4743. doi:10.1073/pnas.1118574109

Peeters, F., Wüest, A., Piepke, G., and Imboden, D. M. 1996. Horizontal mixing in lakes. Journal of Geophysical Research: Oceans, 101(C8), 18361-18375. doi:10.1029/96JC01145

Peeters, F., and H. Hofmann. 2015. Length-scale dependence of horizontal dispersion in the surface water of lakes. Limnology and Oceanography, 60, 1917-1934. doi:10.1002/lno.10141

Poje, A. C., Özgökmen, T. M., Lipphardt, B. L., Haus, B. K., Ryan, E. H., Haza, A. C., ... and Griffa, A. 2014. Submesoscale dispersion in the vicinity of the Deepwater Horizon spill. Proceedings of the National Academy of Sciences, 111(35), 12693-12698. doi: 10.1073/pnas.1402452111

Ralph, E.A., 2002. Scales and structures of large lake eddies. Geophysical research letters, 29(24). doi:10.1029/2001GL014654, 2002

Richardson, L. F. 1926. Atmospheric diffusion shown on a distance-neighbour graph. Proceedings of the Royal Society of London. Series A, 110(756), 709-737. doi:10.1098/rspa.1926.0043

Rowe, M. D., Anderson, E. J., Wynne, T. T., Stumpf, R. P., Fanslow, D. L., Kijanka, K., ... and Davis, T. W. 2016. Vertical distribution of buoyant Microcystis blooms in a Lagrangian particle tracking model for short-term forecasts in Lake Erie. Journal of Geophysical Research: Oceans, 121(7), 5296-5314. doi:10.1002/2016JC011720

Saffman, P. 1962. The effect of wind shear on horizontal spread from an instantaneous ground source. Quarterly Journal of the Royal Meteorological Society, 88(378), 382-393. doi:10.1002/qj.49708837803

Scotti, A. and White, B., 2016. The mixing efficiency of stratified turbulent boundary layers. Journal of Physical Oceanography, 46(10), pp.3181-3191. doi:10.1175/JPO-D-16-0095.1

Stocker, R., and Imberger, J. 2003. Horizontal transport and dispersion in the surface layer of a medium-sized lake. Limnology and Oceanography, 48(3), 971-982. doi:10.4319/lo.2003.48.3.0971

Thomas, L. N., Tandon, A., and Mahadevan, A. 2008. Submesoscale processes and dynamics, in Eddy Resolving Ocean Modeling, Geophys. Monogr. Ser., vol. 177, edited by M. W. Hecht and H. Hasumi, pp. 17–38, AGU, Washington, D. C. doi:10.1029/177GM04

Table

Experiment, time after release	Surface conditions	Fit dispersion coefficient, K (m^2s^{-1}) vs. L (m)	Scale range (L, m)	K range (m^2s^{-1})
Dye, 6-21 hours (present)	Very calm; strongly stratified; NI shear	$K = (2.0x10^{-3})L^{0.97}$	950-2900	1.5 - 4.2
Drifters, 0-5 days (present)	Calm; stratified; NI motions	$K = (3.5x10^{-2})L^{0.2}$	190-1,460 Avg: 0.14 m^2s^{-1}	0.10-0.15
Drifters, 5-24 days (present)	Variable; wind episodes; NI motions	$K = (1.1x10^{-4})L^{1.09}$	1,460-8,000	0.3 – 2.0
Lake Constance Drifters, 3-4 days (PH 2015)	Weakly stratified	$K = (1.27x10^{-4})L^{1.10}$ $K = (0.11x10^{-4})L^{1.61}$ $K = (1.92x10^{-4})L^{1.09}$ $K = (1.08x10^{-4})L^{1.01}$	200-1300 130-3700 100-2000 30-620	0.043-0.33 0.027-5.93 0.027-0.76 0.027-0.07
Lake Ontario Dye (hypolimion), ~4days (Murthy, 1976)		$K = (6.65x10^{-4})L^{1.22}$	324-15261	0.76-83
Oceans Dye, ~24 days (Okubo 1971)	Variable	$K = (3.7x10^{-4})L^{1.20}$	64-110,000	0.054-390
Gulf of Mexico Drifter, ~24 days (Poje et al., 2014)	Variable; NI Motions	$K = (2.68x10^{-4})L^{1.20}$	430-76,000	0.39-190

591

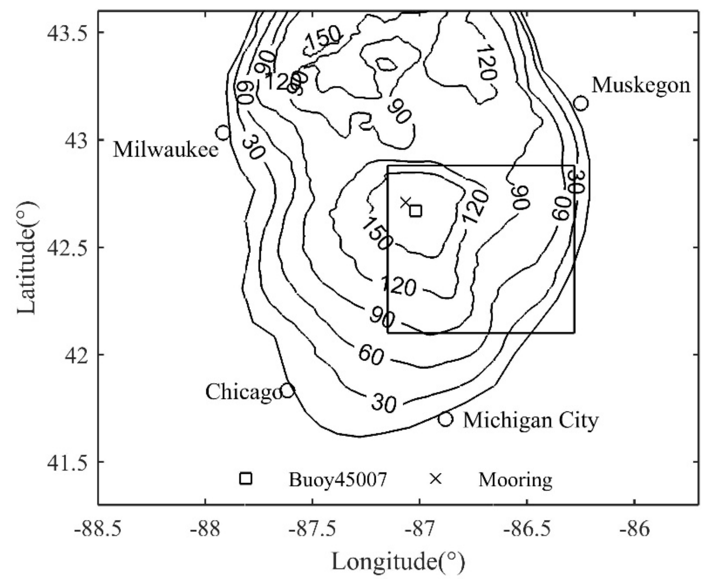

Figure 1. The southern basin of Lake Michigan showing depth contours (m), locations of ADCP and temperature mooring (‘×’), and NDBC (National Data Buoy Center) Buoy 45007 (‘□’). The dye and surface drifters were released within 1 km of the mooring location (‘×’).

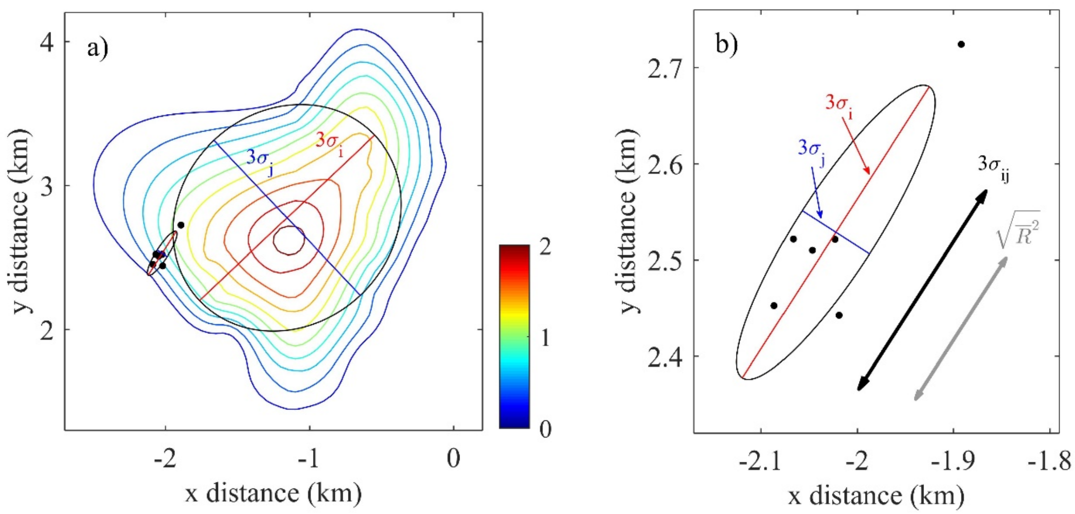

Figure 2. Illustrated definitions of dye patch and drifter cluster dimensions 19 hours after release. a) Concurrent dye patch (contours) and drifter cluster (dots), showing ellipse major ($3\sigma_i$) and minor ($3\sigma_j$) axes dimensions for each. c) Ellipse fitted in drifters shown in b). The length of black and gray lines indicate $3\sigma_{ij}$ and and $\sqrt{R^2}$, respectively. Contour lines in (a) are contours of dye concentration in ppb ranging from 0.2 to 2, in increments of 0.2.

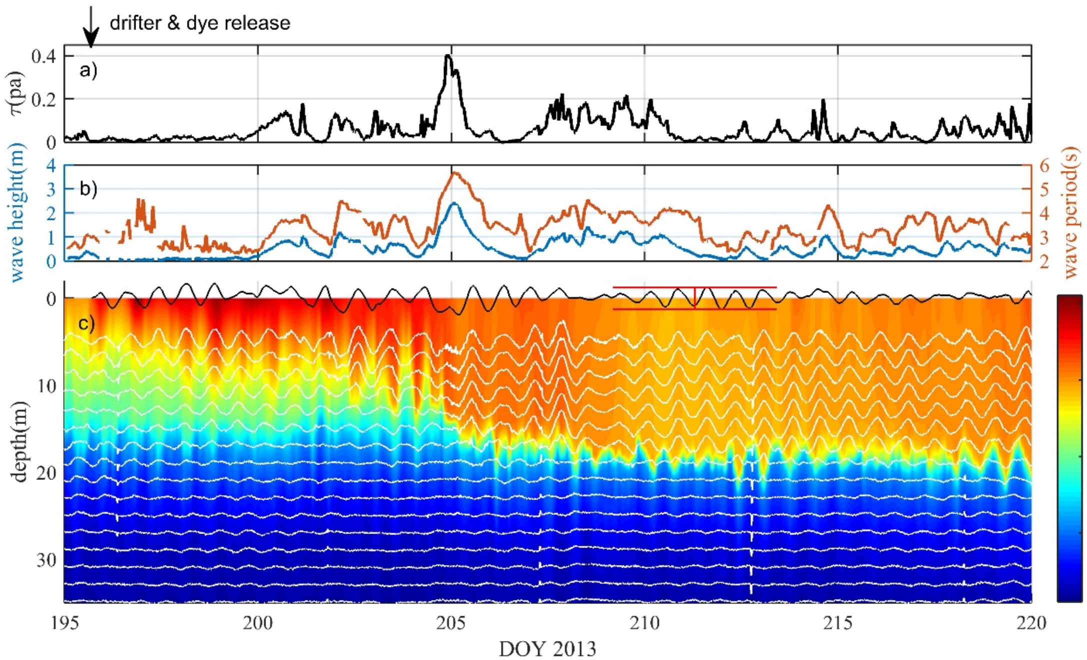

Figure 3. Observations from mid-lake mooring and NDBC Buoy 45007. Shown are (a) wind stress at water surface, (b) wave height and average wave period, and (c) water column currents and temperatures. In plot (c), the east component of ADCP-measured currents is shown as white lines centered at the depths where measured, with 2.5 m of deflection corresponding to 0.5 ms^{-1} indicated by red lines. Also shown at the surface as a black line in (c) is the mean east drifter velocity, obtained by differentiating the mean drifter position with respect to time. Temperatures between 0 - 11 m depths are linearly interpolated.

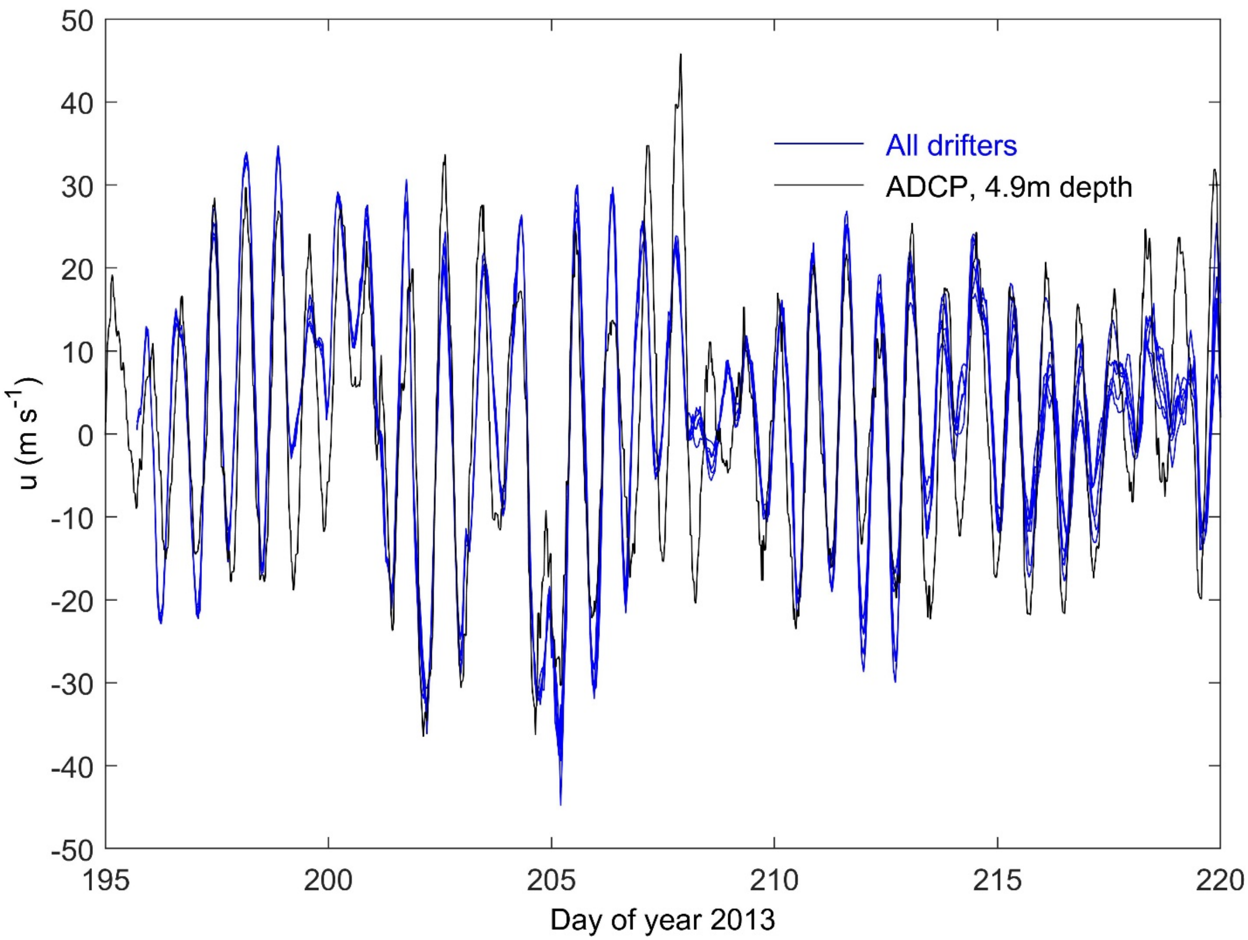

Figure 4. Near-surface ADCP and drifter velocities. Shown are the eastward velocities for all 6 drifters and the nearest-to-surface ADCP measurement (4.9 m depth).

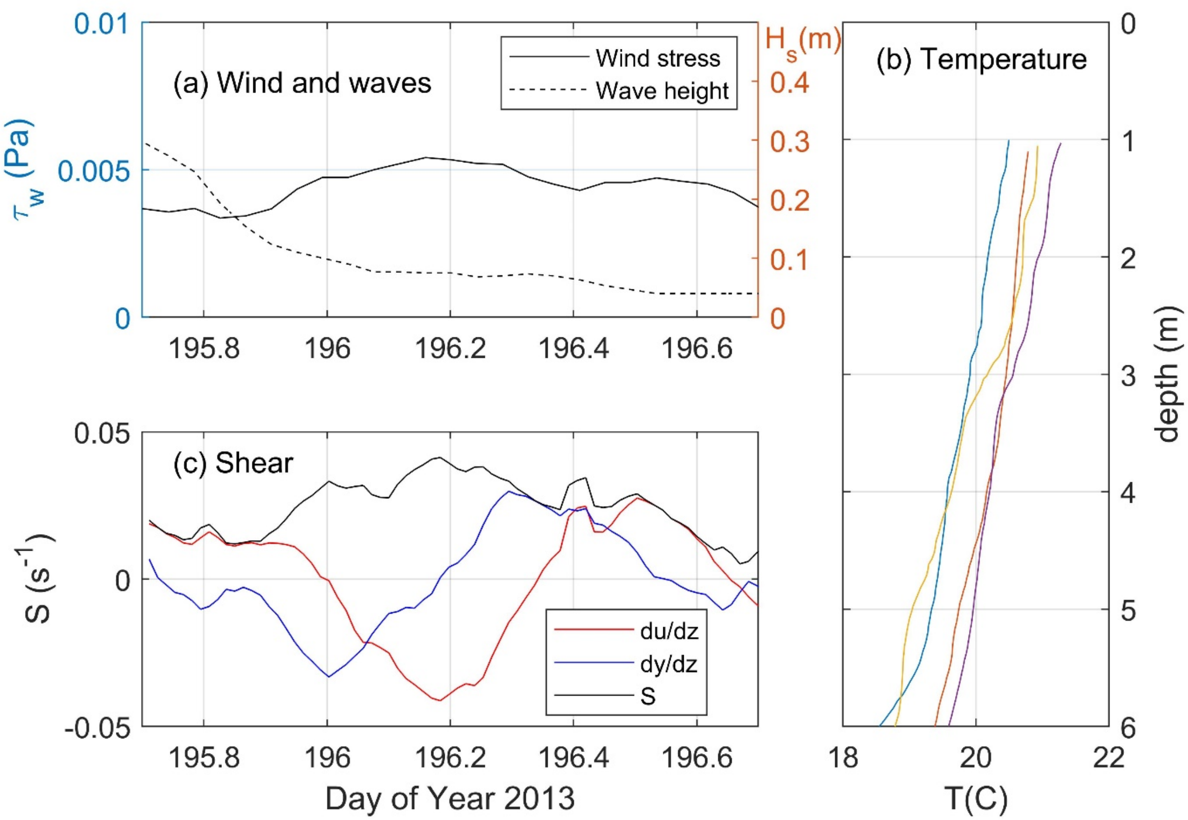

Figure 5. Conditions during the dye release. Shown are (a) estimated wind stress and wave height; (b) near-surface temperature profiles; and (c) estimated shear at depth 2.5 m.

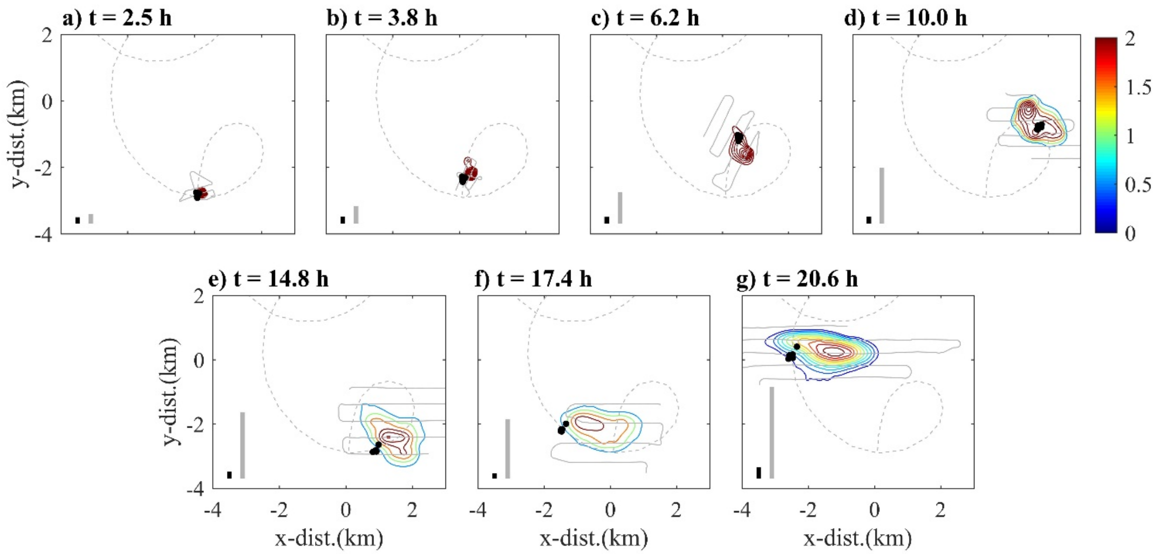

Figure 6. Dye concentration contours at 2 m depth during the 21 h following release. Also shown are ship tracks for particular surveys (gray solid lines) and mean drifter cluster trajectory (gray dashed lines), with drifter positions shown as black circles. Bar graphs at the lower left show corresponding plume lengths $3\sigma_{ij}$ for the drifter cluster (gray) and dye patch (black) inferred from the distributions.

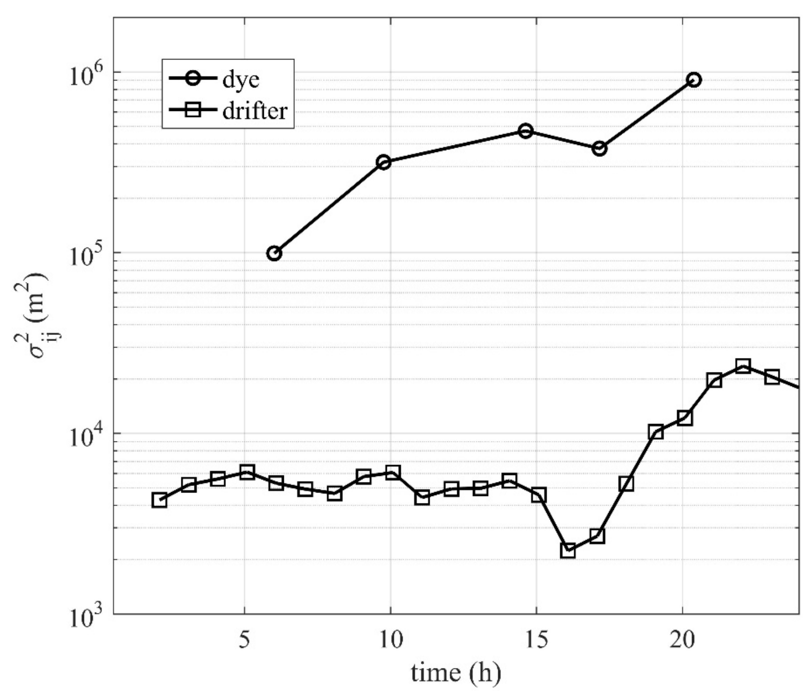

Figure 7. Short-term dispersion during the day-long dye release experiment. Shown are the total variance for dye plume and drifter cluster during the first 24 hours of the experiment following release.

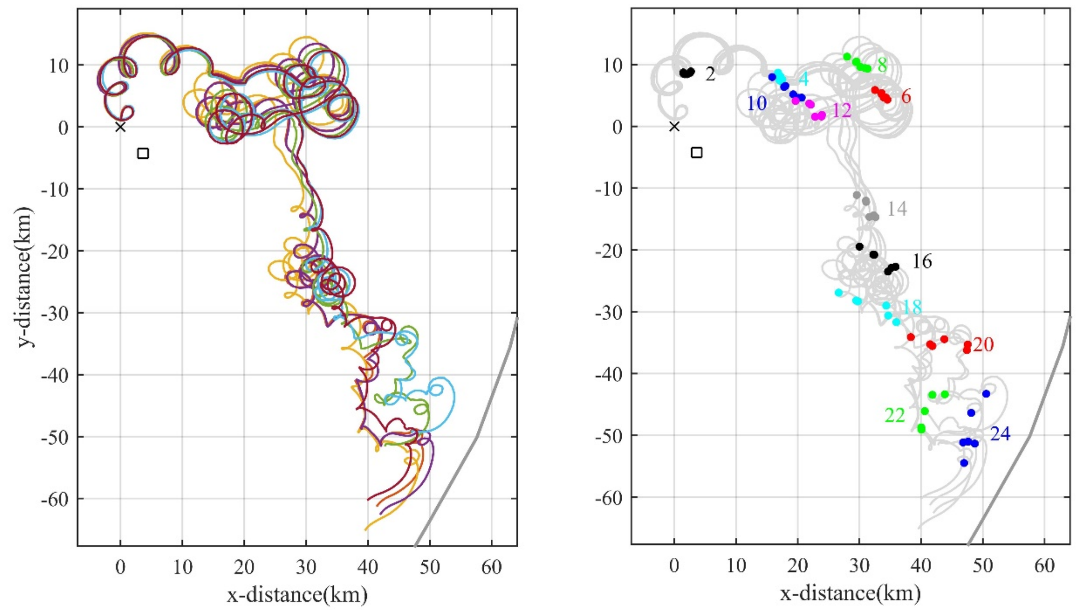

Figure 8. Drifter trajectories for first 25 days of drifter release. Shown are (a) individual drifter trajectories, each with a different color; (b) individual trajectories with markers indicating drifter positions every two days (solid circles with DOY label colored similarly).

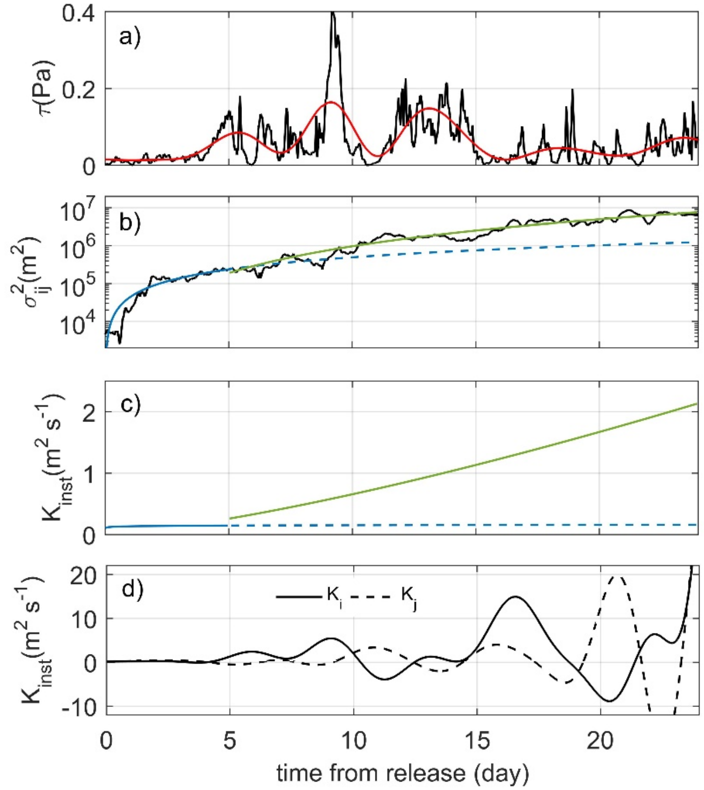

Figure 9. Time series of (a) raw wind stress τ and low-pass filtered (>3days) wind stress; (b) Drifter cluster variance σ_{ij}^2. Best fit power law fits correspond to lines provided in text. (c) Instantaneous dispersion rate $K_{inst} = \frac{1}{4}\frac{d\sigma_{ij}^2}{dt}$ using, fitted lines in b); d) Instantaneous dispersion rates in major (K_i) and minor (K_i) directions.

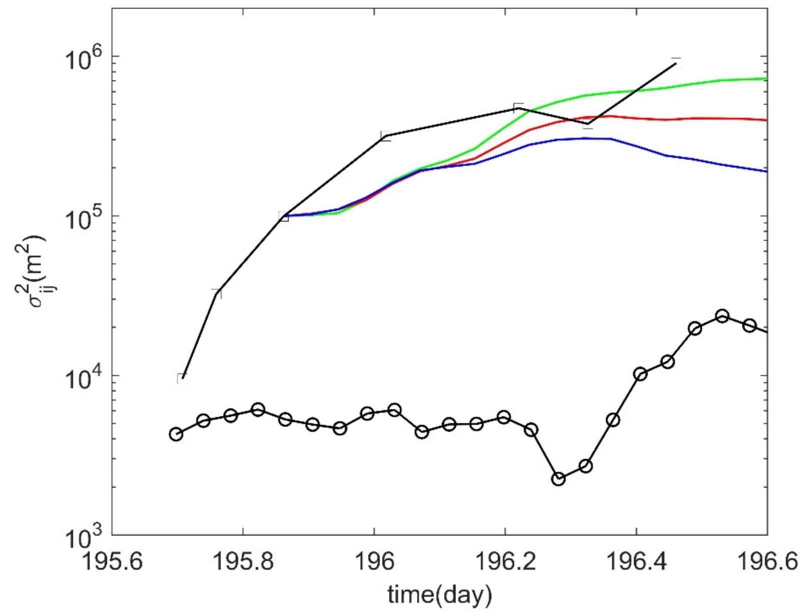

Figure 10. Particle tracking calculations showing potential effect of near-surface vertical shear, relative to measured drifter dispersion (black, circles) and dye dispersion (black, squares). Shown are calculations associated with three vertical mixing rates: 10^{-6} m^2s^{-1} (blue); 10^{-5} m^2s^{-1} (red); 10^{-4} m^2s^{-1} (green). The calculation proceeds from the third measurement of dye variance to avoid potential effects from ship-induced mixing.

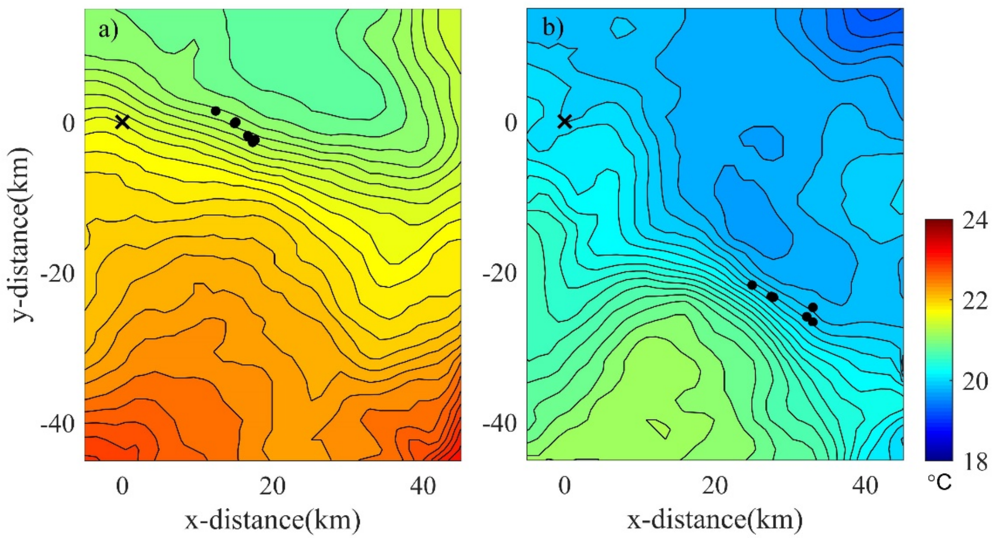

Figure 11. Drifter locations (black dots) embedded in GLSEA SST contour (https://coastwatch.glerl.noaa.gov/) at a) day 11 and b) day 18 from release when thermal front was strong. Interval of contour lines is 0.1°C. Gray lines are drifter trajectories. ‘x’ indicates the location of release adjacent to a mooring.

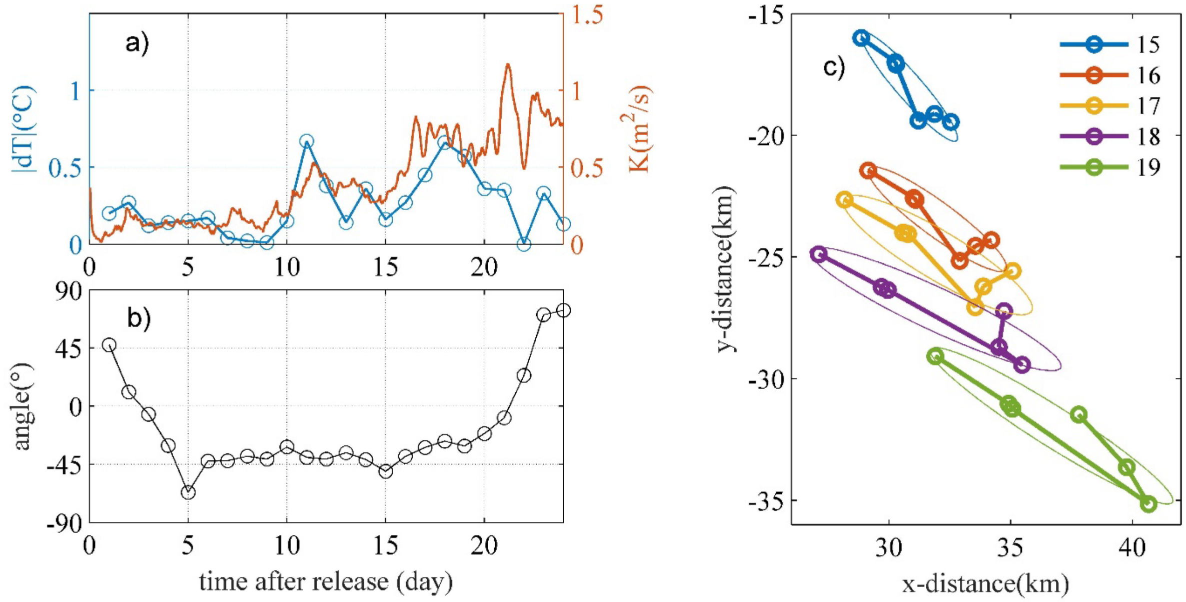

Figure 12. a) Temperature difference ($|dT|$) at thermal front and drifter dispersion coefficient K. dT is defined by temperature difference between two points at edges of 10km transact, centered at center of cluster, perpendicular to major axis; b) angle of major axis produced by 6 drifters respect to E-W axis: c) 18 hours time-averaged drifter locations. All lines are connecting drifters in the same sequence. The lengths of major and minor axes in ellipse are $3\sigma_i$ and $3\sigma_j$.

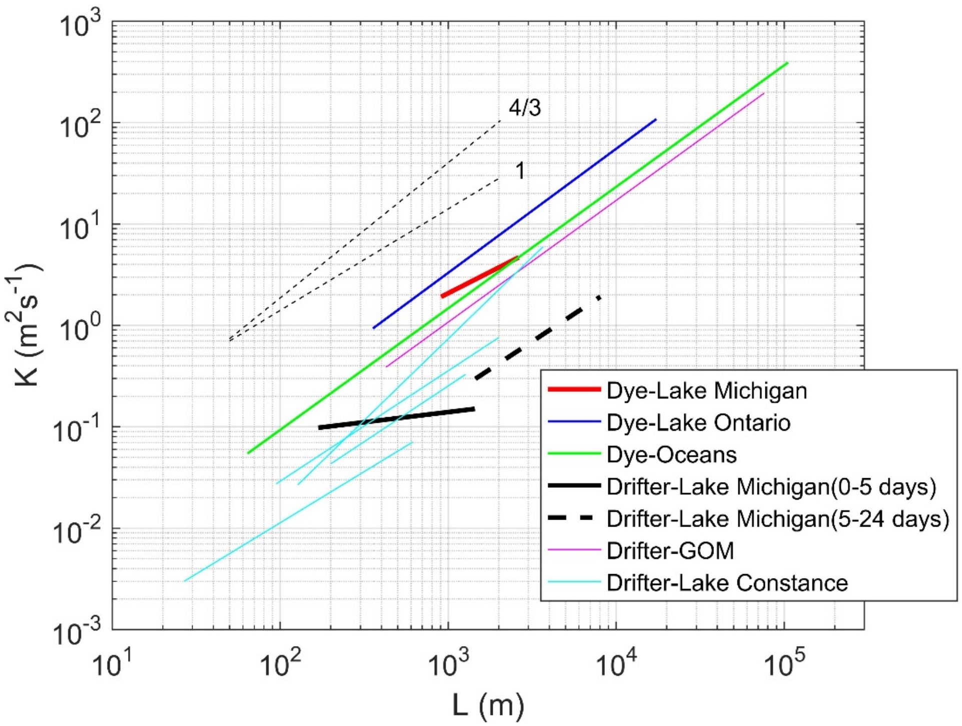

Figure 13. Near-surface dispersion rates vs. cloud size for various systems. Shown are data from Lake Ontario (Murthy 1976), Lake Constance (PH2015), oceans (Okubo 1971), the Gulf of Mexico (GOM) (Poje et al. 2014), and our current results from Lake Michigan.

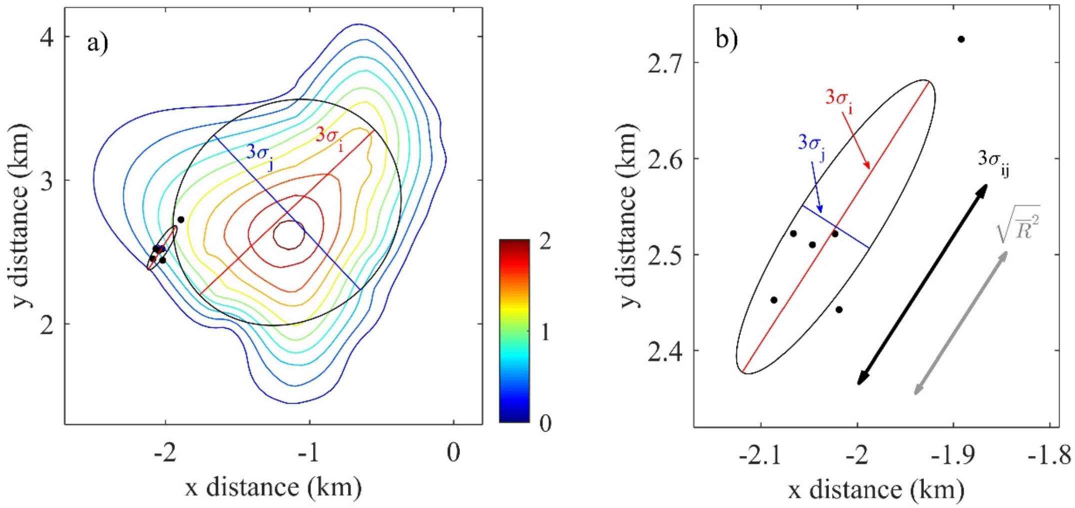

Figure 2. Illustrated definitions of dye patch and drifter cluster dimensions 19 hours after release. a) Concurrent dye patch (contours) and drifter cluster (dots), showing ellipse major ($3\sigma_i$) and minor ($3\sigma_j$) axes dimensions for each. c) Ellipse fitted in drifters shown in b). The length of black and gray lines indicate $3\sigma_{ij}$ and and $\sqrt{\overline{R^2}}$, respectively. Contour lines in (a) are contours of dye concentration in ppb ranging from 0.2 to 2, in increments of 0.2.

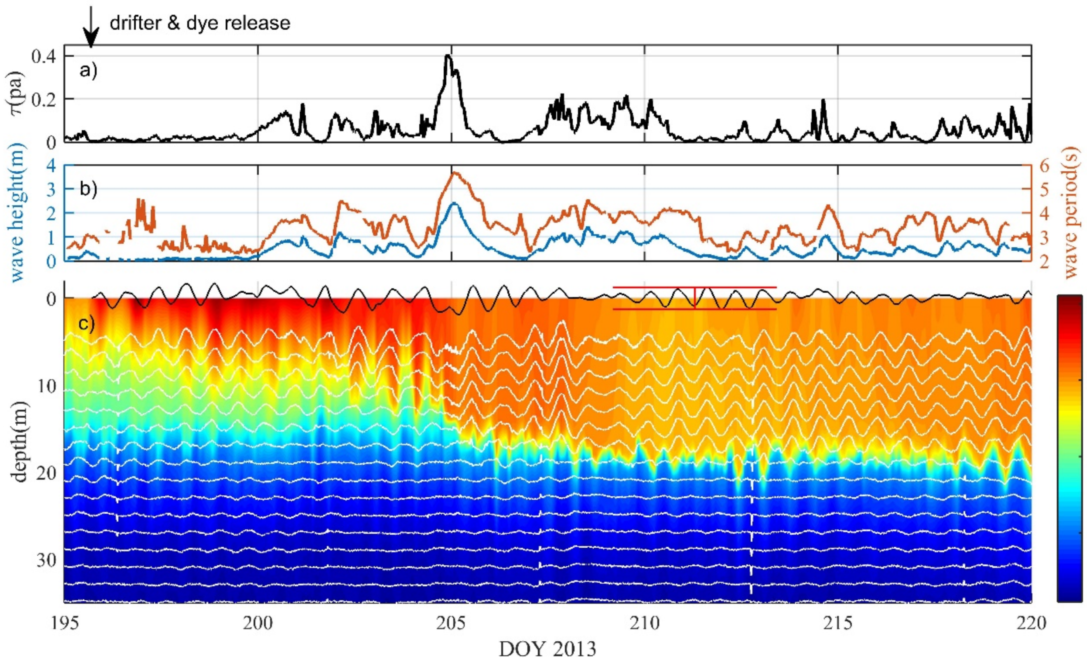

Figure 3. Observations from mid-lake mooring and NDBC Buoy 45007. Shown are (a) wind stress at water surface, (b) wave height and average wave period, and (c) water column currents and temperatures. In plot (c), the east component of ADCP-measured currents is shown as white lines centered at the depths where measured, with 2.5 m of deflection corresponding to 0.5 ms^{-1} indicated by red lines. Also shown at the surface as a black line in (c) is the mean east drifter velocity, obtained by differentiating the mean drifter position with respect to time. Temperatures between 0 - 11 m depths are linearly interpolated.

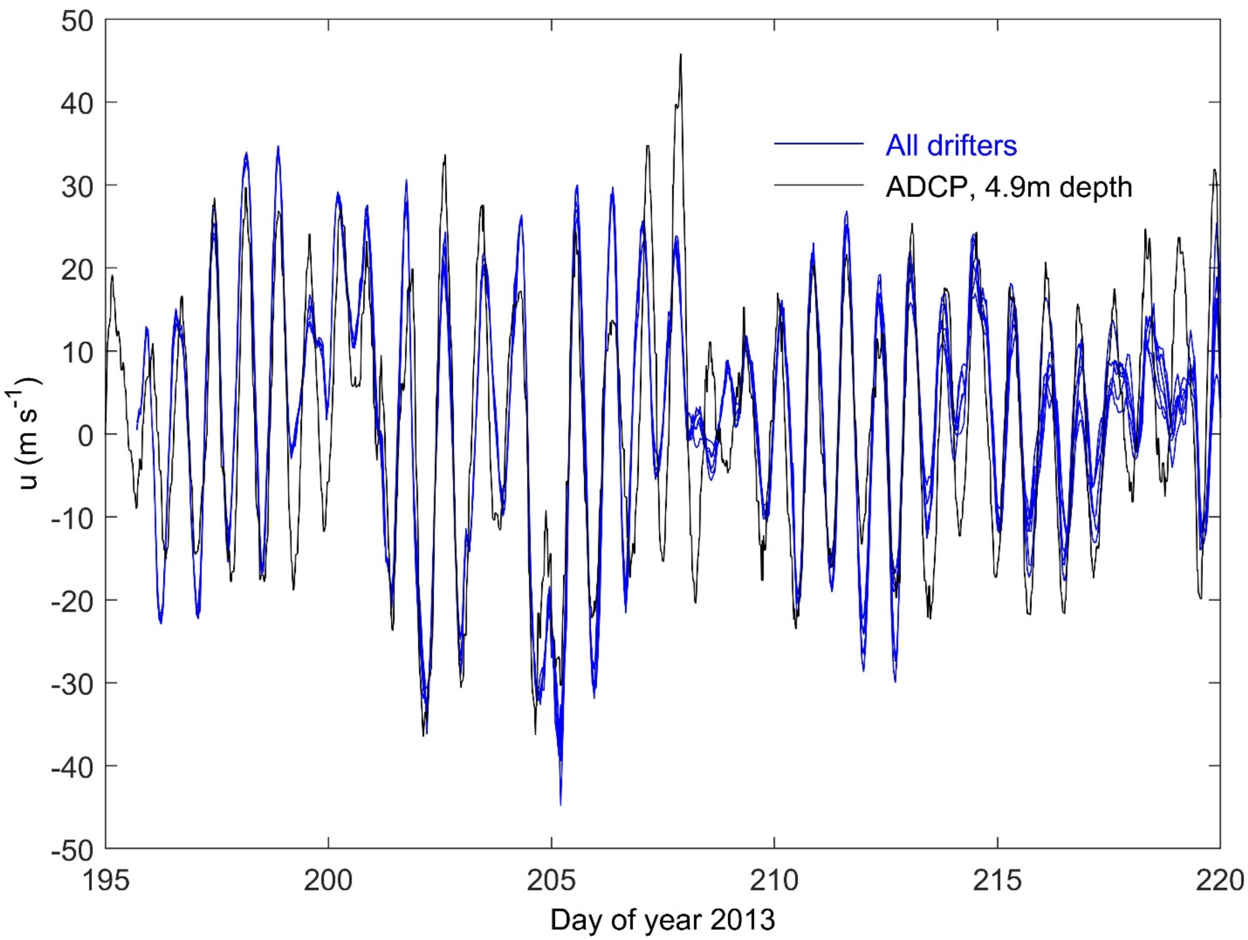

Figure 4. Near-surface ADCP and drifter velocities. Shown are the eastward velocities for all 6 drifters and the nearest-to-surface ADCP measurement (4.9 m depth).

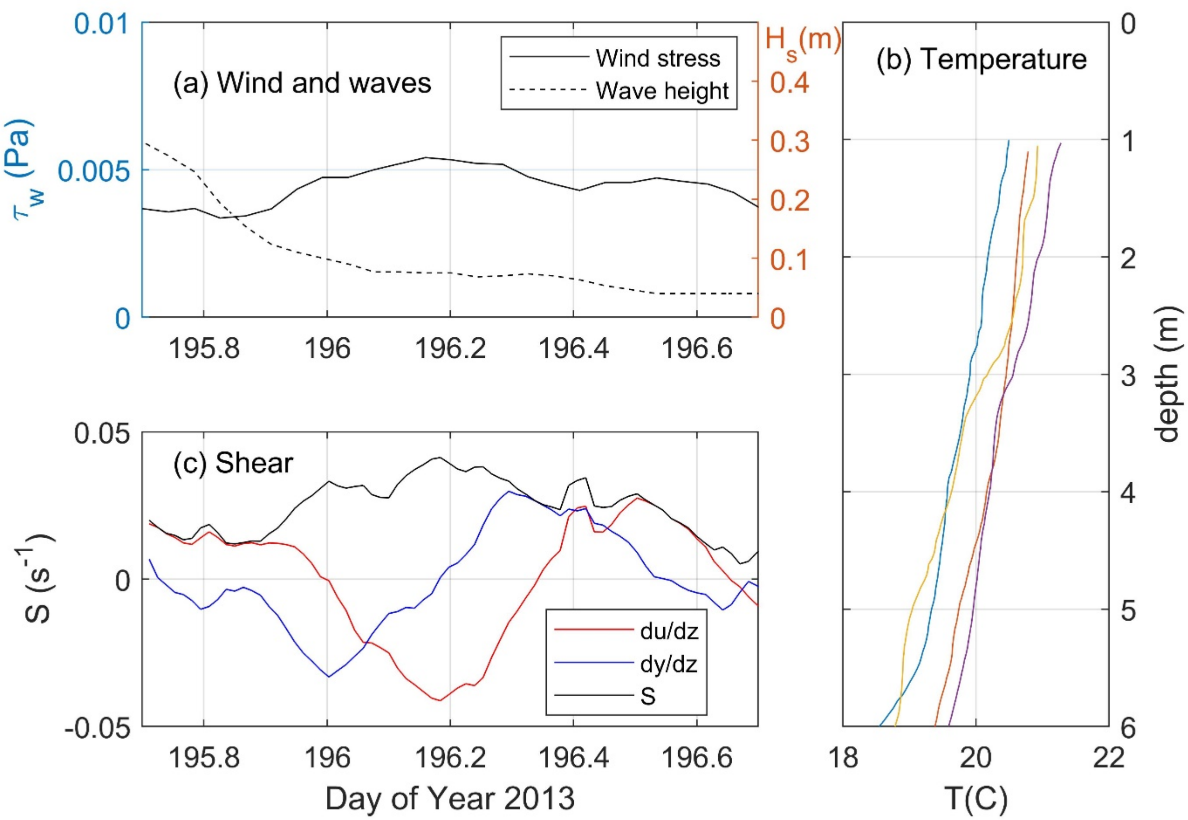

Figure 5. Conditions during the dye release. Shown are (a) estimated wind stress and wave height; (b) near-surface temperature profiles; and (c) estimated shear at depth 2.5 m.

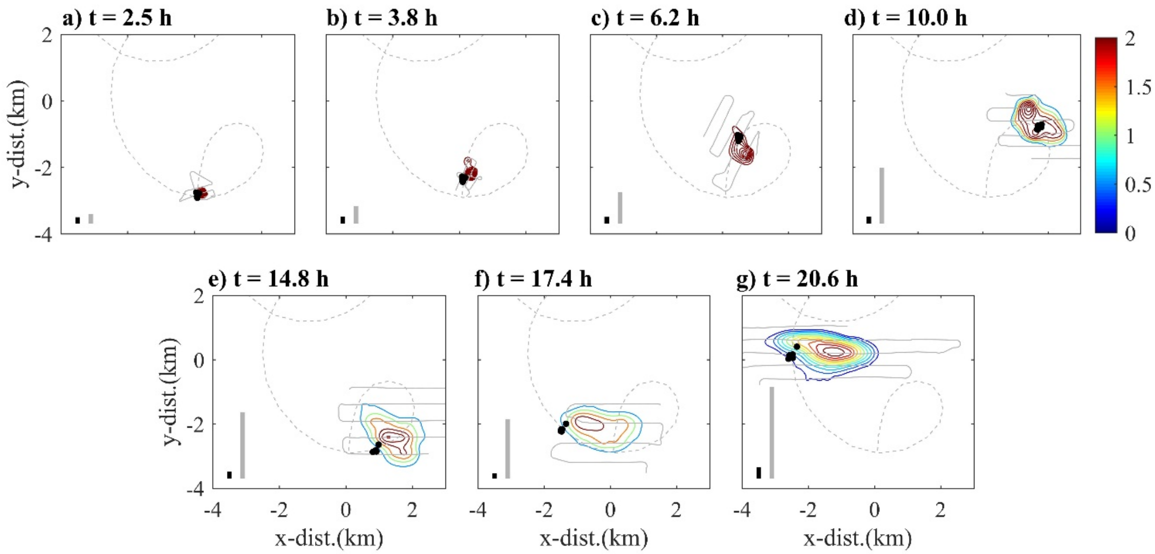

Figure 6. Dye concentration contours at 2 m depth during the 21 h following release. Also shown are ship tracks for particular surveys (gray solid lines) and mean drifter cluster trajectory (gray dashed lines), with drifter positions shown as black circles. Bar graphs at the lower left show corresponding plume lengths $3\sigma_{ij}$ for the drifter cluster (gray) and dye patch (black) inferred from the distributions.

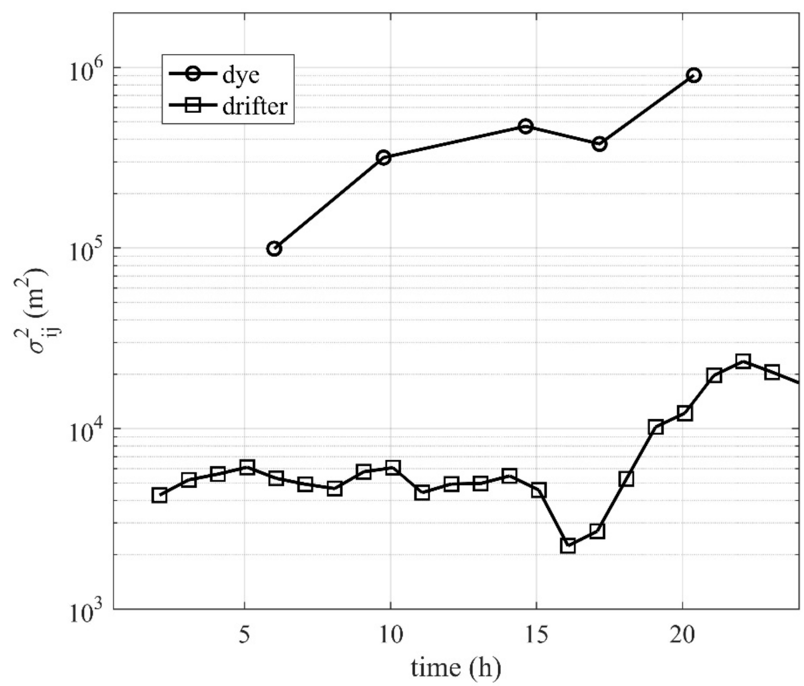

Figure 7. Short-term dispersion during the day-long dye release experiment. Shown are the total variance for dye plume and drifter cluster during the first 24 hours of the experiment following release.

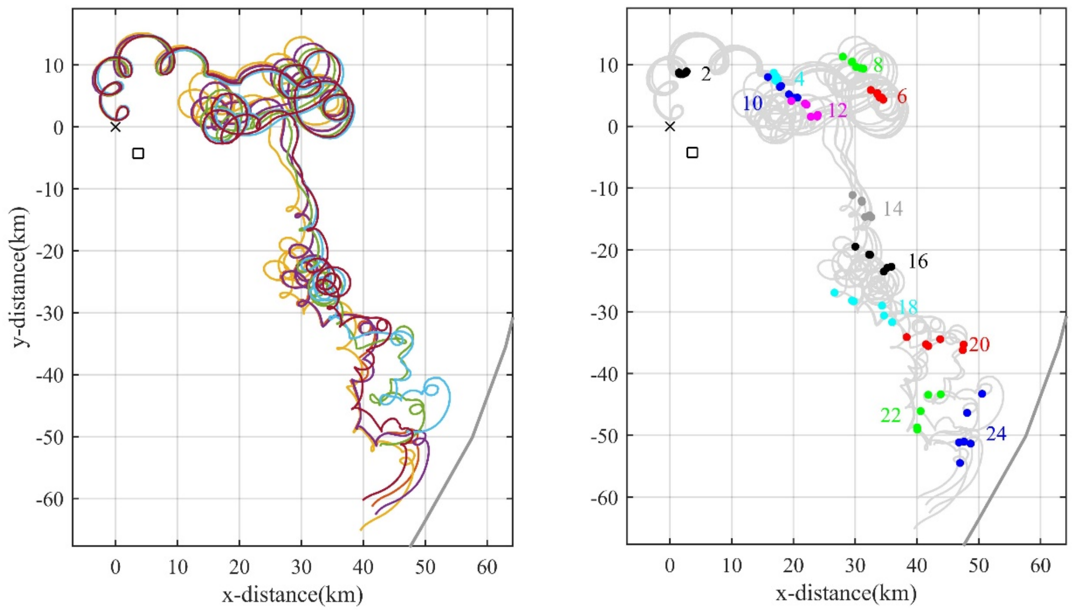

Figure 8. Drifter trajectories for first 25 days of drifter release. Shown are (a) individual drifter trajectories, each with a different color; (b) individual trajectories with markers indicating drifter positions every two days (solid circles with DOY label colored similarly).

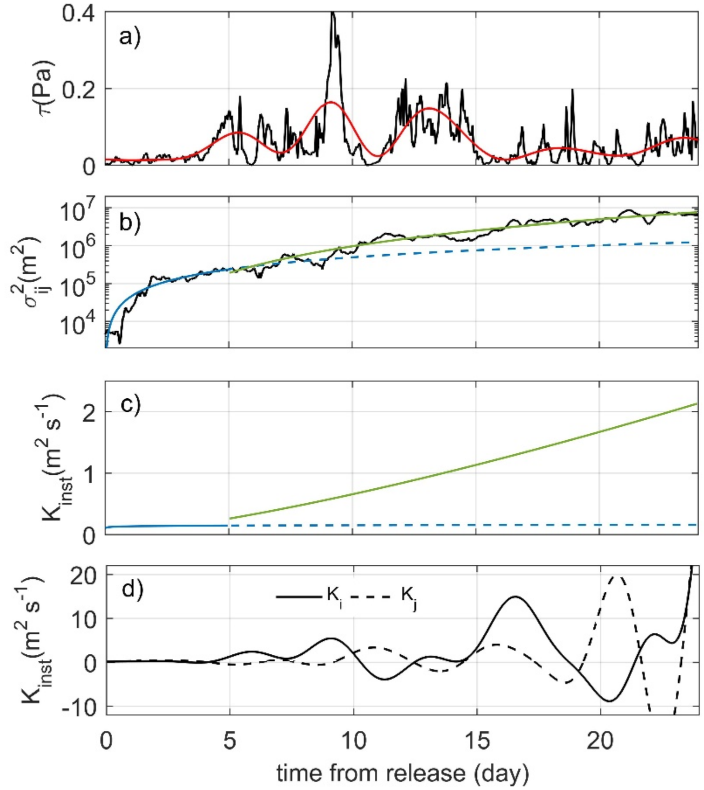

Figure 9. Time series of (a) raw wind stress τ and low-pass filtered (>3days) wind stress; (b) Drifter cluster variance σ_{ij}^2. Best fit power law fits correspond to lines provided in text. (c) Instantaneous dispersion rate $K_{inst} = \frac{1}{4}\frac{d\sigma_{ij}^2}{dt}$ using, fitted lines in b); d) Instantaneous dispersion rates in major (K_i) and minor (K_i) directions.

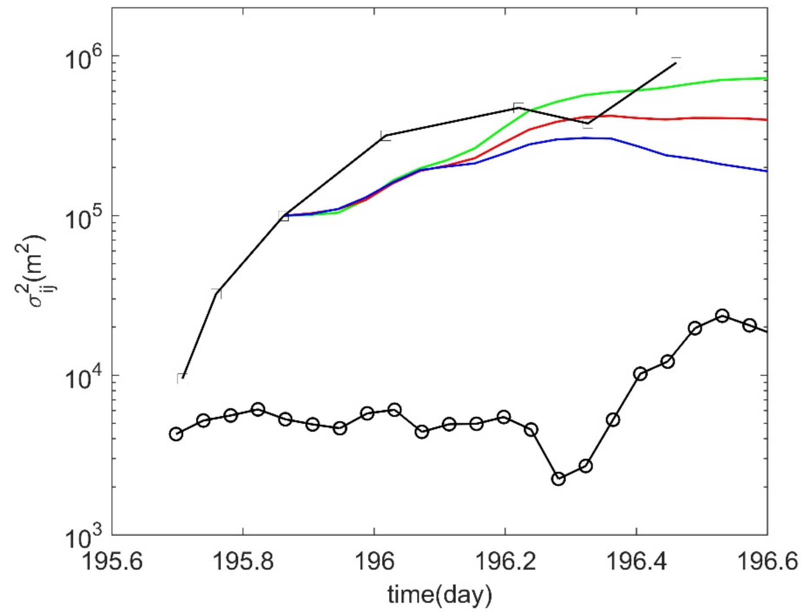

Figure 10. Particle tracking calculations showing potential effect of near-surface vertical shear, relative to measured drifter dispersion (black, circles) and dye dispersion (black, squares). Shown are calculations associated with three vertical mixing rates: 10^{-6} m^2s^{-1} (blue); 10^{-5} m^2s^{-1} (red); 10^{-4} m^2s^{-1} (green). The calculation proceeds from the third measurement of dye variance to avoid potential effects from ship-induced mixing.

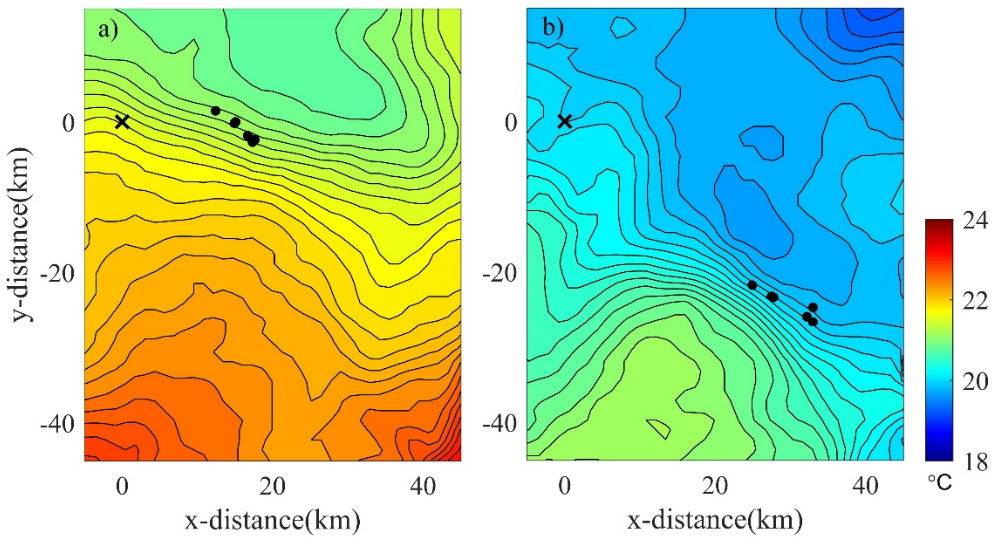

Figure 11. Drifter locations (black dots) embedded in GLSEA SST contour ([https://coastwatch.glerl.noaa.gov/)](https://coastwatch.glerl.noaa.gov/) at a) day 11 and b) day 18 from release when thermal front was strong. Interval of contour lines is 0.1°C. Gray lines are drifter trajectories. ‘x’ indicates the location of release adjacent to a mooring.

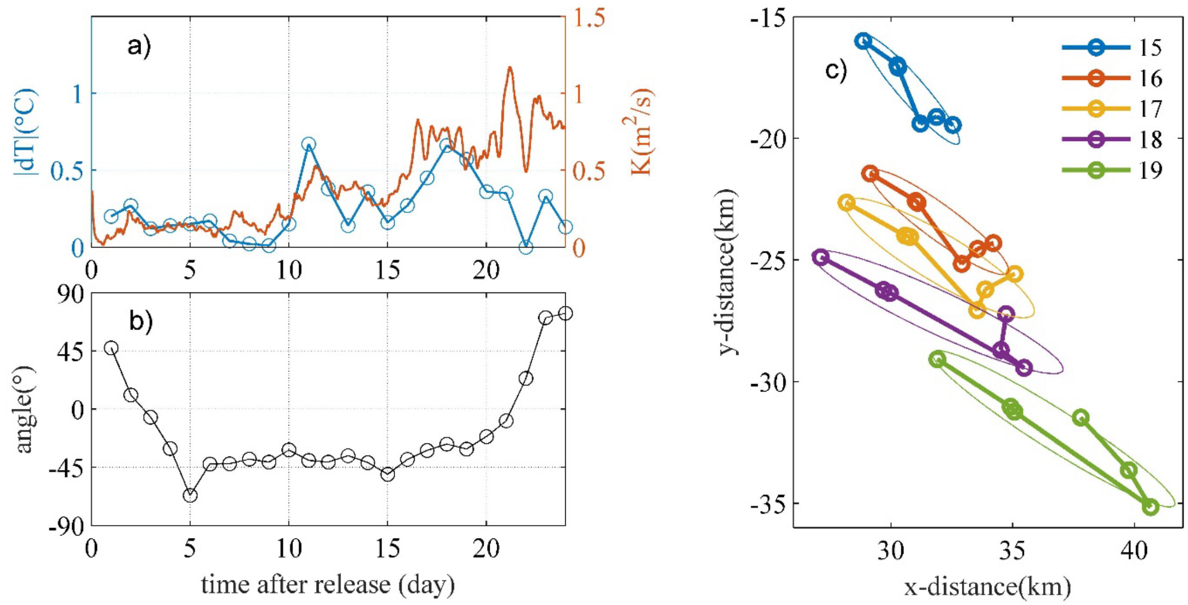

Figure 12. a) Temperature difference ($|dT|$) at thermal front and drifter dispersion coefficient K. dT is defined by temperature difference between two points at edges of 10km transact, centered at center of cluster, perpendicular to major axis; b) angle of major axis produced by 6 drifters respect to E-W axis: c) 18 hours time-averaged drifter locations. All lines are connecting drifters in the same sequence. The lengths of major and minor axes in ellipse are $3\sigma_i$ and $3\sigma_j$.

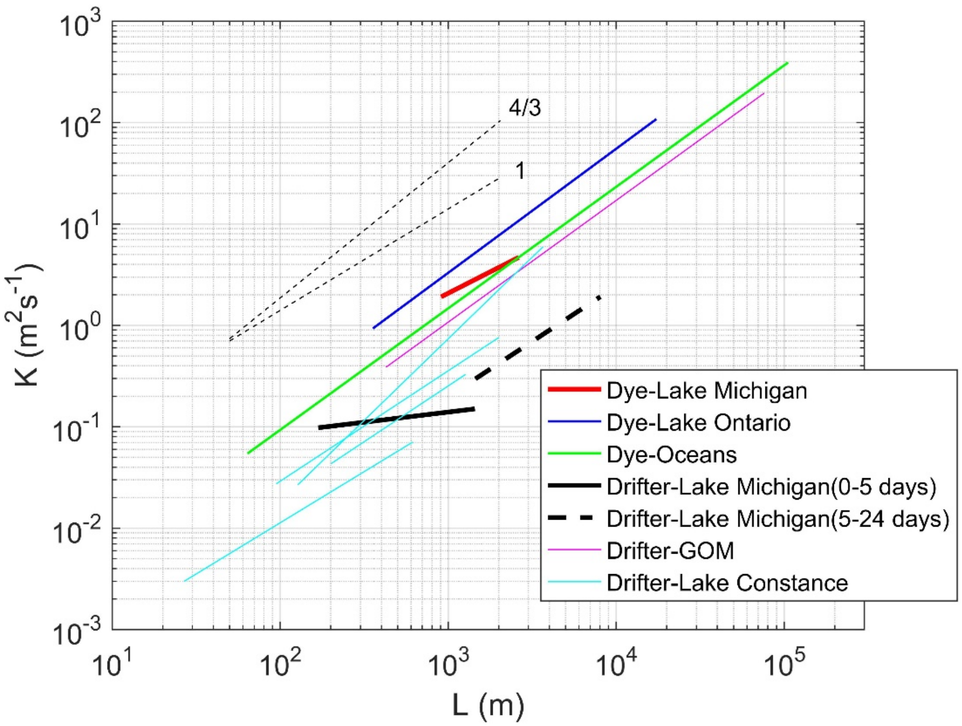

Figure 13. Near-surface dispersion rates vs. cloud size for various systems. Shown are data from Lake Ontario (Murthy 1976), Lake Constance (PH2015), oceans (Okubo 1971), the Gulf of Mexico (GOM) (Poje et al. 2014), and our current results from Lake Michigan.